X-ray-scattering studies of the interfacial structure of Au/GaAs

D. Y. Noh
Exxon Corporate Research Laboratory, Annandale, New Jersey 08801

Y. Hwu
Institute of Physics, Academia Sinica, Taipei, Taiwan

H. K. Kim
Department of Physics, Pusan National University, Pusan, Korea

M. Hong
AT&T Bell Laboratories, Murray Hill, New Jersey 07974
(Received 23 August 1994)

We present results of an x-ray-reflectivity measurement on a Au film, 1000-Å thick, *in situ* epitaxially grown on GaAs by molecular-beam epitaxy. Roughness of both air/Au and Au/GaAs interfaces was obtained from the specular-reflectivity curve. Interfacial height fluctuations of the air/Au interface were found to be correlated to those of the Au/GaAs interface. The correlation of the height fluctuations was obtained quantitatively from the diffuse scattering profile. Satellite peaks in the rocking curves at small incident angles were also observed and attributed to the correlated roughness and to the dynamic scattering effects. Upon heating the sample to 400 °C, the interface became rougher and the interfacial correlation was lost. We speculate that the interfacial changes were caused by interdiffusion at elevated temperatures.

I. INTRODUCTION

Epitaxially grown Au films on semiconductor substrates, especially on GaAs surfaces have a wide variety of applications in the semiconductor industry. The interfacial structure of such systems is believed to play a major role in determining electronic properties such as resistivity and Schottky barrier height.[1,2] It has been rather difficult to apply modern electron microscopes such as scanning tunneling microscopy and transmission electron microscopy in studying the interfacial structure since the interface is buried under an overlayer film. The objective of this study is to demonstrate the capability of x-ray scattering in studying the interface structure nondestructively using a model system, Au/GaAs.

The usefulness of x-ray reflectivity in studying surface roughness has been demonstrated,[3] and applied to various systems.[4,5] The behavior of the specular reflectivity, where the exit and the incident angles of x rays with respect to a surface are equal, is directly related to the rms of the surface roughness. Meanwhile, surface height fluctuations are manifested in the diffuse scattering profile around the specular-reflectivity rod. The detailed scattering cross section was well documented in a classic paper by Sinha *et al.*[6] Recently, there are also great theoretical and experimental efforts to utilize the x-ray reflectivity in studying interfaces of multilayer systems.[7–9] With the unique penetrating power, x rays are ideal probes to study the structure of interfaces buried under overlayers. Although the scattering cross section of buried interfaces can be quite complicated to be of any use, it is now believed that one might obtain the roughness of each interface and the correlation between the interfaces from the reflectivity measurement.

The interfacial structure can be described by a height-fluctuation function, $G_{ij}(r)\equiv\langle[h_i(\mathbf{r})-h_j(0)]^2\rangle$, where $h_i(\mathbf{r})$ represents the height variation of the ith interface at lateral position $\mathbf{r}$ in the film plane from the mean height. Here the statistical average is to be considered as a configurational average rather than a thermal average because the fluctuations in a multilayer film are usually frozen. The rms roughness or the interface width of the ith interface, $\sigma_i\equiv\sqrt{\langle h_i^2(\mathbf{r})\rangle}$ is related to the fluctuation function by $G_{ii}(\infty)=2\sigma_i^2$. At the origin, the fluctuation function across interfaces attains a finite value $[\lim_{r\to 0} G_{ij}(\mathbf{r})\neq 0\ (i\neq j)]$, since interfaces are not usually perfectly correlated. Many properties of a multilayer film depend not only on the interface width σ_i, but also on the details of $G_{ij}(\mathbf{r})$. $G_{ij}(\mathbf{r})$ is a good measure of the propagation of interface height fluctuations due to defects such as steps and islands through overlayer films. In an x-ray diffraction experiment, we measure a Fourier transform of $G_{ij}(r)$ as will be clear in the following sections.

In this paper, we demonstrate the usefulness of the x-ray reflectivity in analyzing the interfacial structure of an Au film grown on GaAs by molecular-beam epitaxy (MBE). The roughness of both interfaces, $\sigma_1=\sqrt{\langle h_1^2(\mathbf{r})\rangle}$ (air/Au) and $\sigma_2=\sqrt{\langle h_2^2(\mathbf{r})\rangle}$ (Au/GaAs) was obtained from the x-ray-specular-reflectivity curve. The height fluctuations of the air/Au interface were correlated to those of the Au/GaAs interface as indicated by the intensity oscillations in the diffuse scattering. The correlation between the height fluctuations across the interfaces, $G_{12}(r)=\langle[h_2(r)-h_1(0)]^2\rangle$ was obtained quanti-

0163-1829/95/51(7)/4441(8)/$06.00

tatively by analyzing the diffuse scattering profile around the specular rod. In addition, we found interesting satellite peaks in the rocking curves at small q_z (momentum transfer along the surface normal) values. These peaks were found to be a combined result of the rapid intensity oscillations in the diffuse scattering due to the interfacial correlation and of often ignored dynamic scattering effects at small incident angles.

Upon heating the sample to 400 °C, the interfacial structure was modified greatly. As was obvious from the specular reflectivity of the annealed sample, the Au/GaAs interface was much less well defined than that of the as-grown sample. The interfacial correlation was also greatly reduced. We attribute the modification of the reflectivity curve to the interdiffusion of Au and GaAs atoms across the interface. The small modulation in the reflectivity curve indicated that the thickness of the interdiffused layer was about 60 Å.

This paper is organized as follows. In Sec. II we describe the film preparation, x-ray measurement setup, and a brief crystallographic information of the Au overlayer film. In Sec. III, we discuss the specular-reflectivity measurement. A brief review of the scattering cross section is presented to aid in understanding the data. In Sec. IV, we discuss the correlation between the height fluctuations of the two interfaces. A scheme to obtain the quantitative correlation function is elaborated. In Sec. V, we present the satellite peaks in the rocking curves at small incident angles. In Sec. VI, the changes in the interfacial structure upon annealing are discussed. We summarize our results in Sec. VII.

II. EXPERIMENTAL DETAILS

A. Experimental setup

The measurement was performed at Beamline X10B at the National Scynchrotron Light Source. The incident x rays were focused vertically by a focusing mirror. A horizontally bent Si(111) crystal was used to monochromatize x rays to 11 keV, and to focus them horizontally as well. For the detector resolution, we used a Ge(111) analyzer crystal to achieve a high-resolution configuration in the plane of scattering. The longitudinal resolution Δq_z thus achieved was 8×10^{-4} Å^{-1} (HWHM is the half width at the half maximum), and the transverse resolution Δq_x in the scattering plane was 5×10^{-5} Å^{-1} (HWHM) at $q_z=0.25$ Å^{-1}. Out of the scattering plane, in q_y direction, the resolution was controlled by two pairs of slits that were left wide open to achieve an automatic integration of the scattering intensity in the corresponding direction. A schematic illustration of the scattering geometry used in this experiment is shown in Fig. 1. During the x-ray measurement, the sample was kept in a x-ray chamber that was evacuated to 1×10^{-5} torr to protect the sample surface from any contamination, especially when it was heated up.

The Au/GaAs sample was prepared in the multiple-chamber system that included a solid-source GaAs-based MBE and a metal MBE.[10] The two chambers are linked together by transfer modules with a pressure of 5×10^{-11} torr. Before depositing Au, we deposited 0.5–1.0 μm of GaAs buffer layers on a commercial GaAs (001) substrate to make an As-stabilized GaAs surface using standard growth parameters. The sample was then transferred to the arsenic-free metal MBE chamber without being exposed to air. Here, Au with a thickness of 1000 Å was evaporated from a effusion cell. The substrate temperature during the metal deposition was held to around 100 °C to prevent any interdiffusion between the GaAs and the Au.

B. Crystallographic information

Prior to the reflectivity measurement, we measured a few Au Bragg peaks to obtain crystallographic information of the Au film. Surprisingly, the Au film was grown along the $\langle 110\rangle_{Au}$ direction rather than along the stable $\langle 001\rangle_{Au}$ direction. In the film plane, the $\langle 1\bar{1}0\rangle_{Au}$ direction was aligned to the $\langle 110\rangle_{GaAs}$ direction of the GaAs substrate, while the $\langle 001\rangle_{Au}$ was parallel to the $\langle 1\bar{1}0\rangle_{GaAs}$. Although the GaAs substrate has a fourfold symmetry in its structure, we observed only domains with $\langle 1\bar{1}0\rangle_{Au}\|\langle 110\rangle_{GaAs}$. No domains with $\langle 1\bar{1}0\rangle_{Au}\|\langle 1\bar{1}0\rangle_{GaAs}$ were observed. These results are rather surprising considering that the lattice mismatch between the Au (lattice constant of 4.078 Å) and the

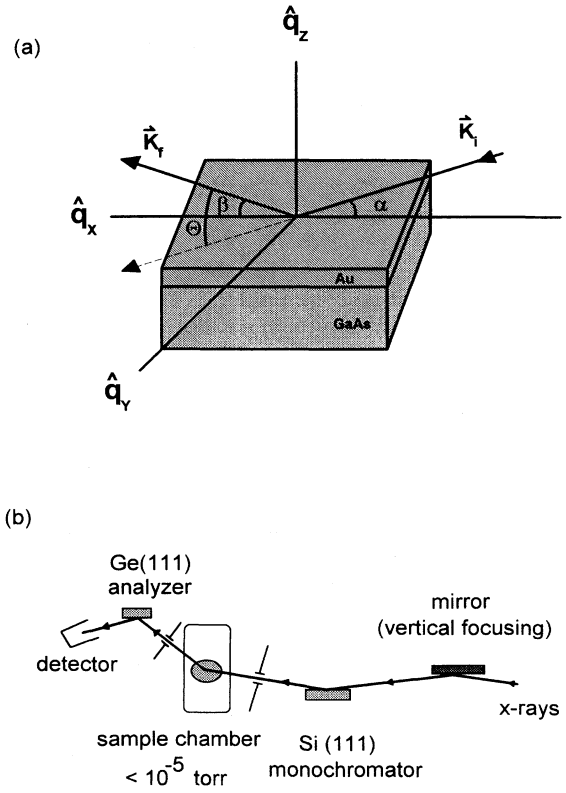

FIG. 1. (a) The reciprocal-lattice coordinate system relative to the sample normal, and the incident and exiting directions of x rays. (b) Experimental geometry used in this experiment. The vertical scattering geometry was used while the monochromator reflected x rays horizontally.

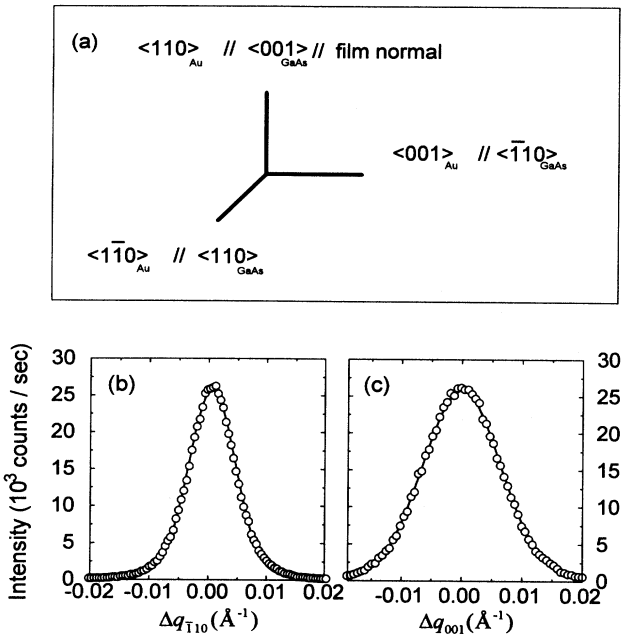

FIG. 2. (a) The crystalline axes direction of Au relative to that of GaAs. (b) Scattering profile of the Au (200) Bragg peak along the $\langle \bar{1}10 \rangle_{Au}$ direction, and (c) along the $\langle 001 \rangle_{Au}$ direction. The solid lines are the best fits to a Gaussian profile.

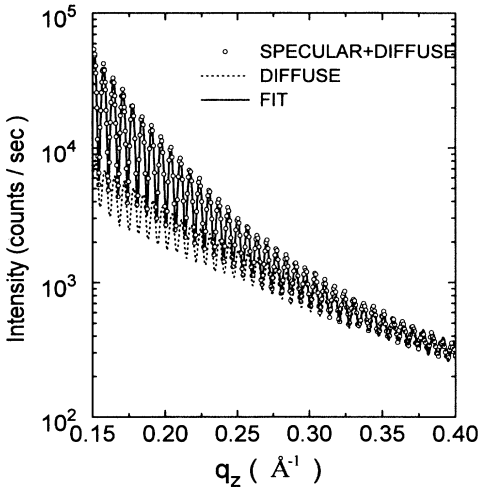

FIG. 3. Specular-reflectivity curve that shows regular intensity oscillations. The solid line is a result of fit to Eq. (2) as described in the text. The broken line is the measured intensity of the diffuse scattering along q_z at $q_x=0.0003$ Å^{-1}, $q_y=0$ Å^{-1}. The intensity oscillations in the diffuse scattering showed that the height fluctuations of the two interfaces were correlated.

GaAs (lattice constant 5.653 Å) could be minimized when the Au grows along the $\langle 001 \rangle_{Au}$ direction keeping the in-plane orientation matched; $\langle 110 \rangle_{Au} \| \langle 100 \rangle_{GaAs}$, $\langle 1\bar{1}0 \rangle_{Au} \| \langle 010 \rangle_{GaAs}$. We suspect that the directional nature of the covalent bonds of GaAs might have significant effects on the crystalline direction of the Au overlayer. Further study of the local electronic properties at the interface is required to elucidate the observed crystalline structure. In Fig. 2(a), the relative crystalline axes direction of the Au and the GaAs was illustrated.

To obtain the in-plane crystal domain size of the Au film, we measured the line profile of the Au (200) Bragg peak. As illustrated in Fig. 2(b), the peak width was anisotropic, 0.0048 Å^{-1} (HWHM) in the $\langle \bar{1}10 \rangle_{Au}$ direction, and 0.0078 Å^{-1} (HWHM) in the $\langle 001 \rangle_{Au}$ direction. This indicates that the in-plane crystal domain size, calculated by $\sim \pi$/HWHM, was anisotropic; 400-Å wide in the $\langle 001 \rangle_{Au}$ direction, and about 650-Å long in the $\langle \bar{1}10 \rangle_{Au}$ direction. We speculate that the anisotropic domain size may be related to the anisotropic lattice mismatch. The lattice mismatch along the $\langle \bar{1}10 \rangle_{Au}$ direction is about 27%, while along the $\langle 001 \rangle_{Au}$ direction, the lattice mismatch is only 2.0%. The mosaic distribution of the film surface normal, $\langle 110 \rangle_{Au}$ axis, was less than 0.01° (HWHM), which was excellent for the reflectivity measurement using the high-resolution configuration involved in this experiment.

III. SCATTERING CROSS SECTION AND THE SPECULAR REFLECTIVITY

As illustrated in Fig. 3, the specular reflectivity measured on the as-grown sample showed the characteristic intensity oscillations from a finite-sized overlayer film. The data were taken along the q_z direction keeping the in-plane momentum transfer fixed to zero, $q_x=q_y=0$. The regular intensity oscillations were originated from the finite nature of the Au film thickness, and indicated that the overlayer was quite uniform in thickness. From the period of oscillations δq_z, we estimate the film thickness given by $2\pi/\delta q_z$ to be 960±5 Å. This agrees well with the measured thickness in the MBE growth process. The decay of the overall intensity and the amplitude of the oscillations in the specular-reflectivity curve provides crucial information on the roughness of both the air/Au and Au/GaAs interfaces.

To describe the reflectivity quantitatively, we extended the scattering cross section derived in a kinematic approximation by Sinha *et al.*[6] to include contributions from both interfaces,

$$S(\mathbf{q}) \approx \frac{1}{q_z^2} \int d\mathbf{r} [\rho_1^2 e^{(q_z^2/2)G_{11}(\mathbf{r})} + (\rho_1-\rho_2)^2 e^{-(q_z^2/2)G_{22}(\mathbf{r})} + 2\rho_1(\rho_1-\rho_2)\cos(q_z d) e^{-(q_z^2/2)G_{12}(\mathbf{r})} e^{-q_z^2\delta^2}] e^{i\mathbf{q}_\perp \mathbf{r}}, \quad (1)$$

where ρ_1 (ρ_2) is the electron density of Au (GaAs), d is the average film thickness, δ is the rms deposition error across the illuminated area of the sample, the $G_{ij}(\mathbf{r})$ is the height-fluctuation function. We used $\mathbf{r}$ to represent the lateral real-space coordinate in the film plane, and $\mathbf{q}_\perp$ to represent the momentum transfer in the film plane. Equation (1) can readily be decomposed into a specular and a diffuse part,[7,9]

$$S_{\text{spec}}(\mathbf{q})=\frac{A}{q_z^2}[\rho_1^2 e^{-q_z^2\sigma_1^2}+(\rho_1-\rho_2)^2 e^{-q_z^2\sigma_2^2}+2\rho_1(\rho_1-\rho_1)\cos(q_z d)e^{-q_z^2(\sigma_1^2+\sigma_2^2+\delta^2)}]\delta(\mathbf{q}_\perp)\ , \tag{2}$$

$$S_{\text{diff}}(\mathbf{q})=\frac{A}{q_z^2}\int d\mathbf{r}\{\rho_1^2 e^{-q_z^2\sigma_1^2}[\exp(q_z^2 C_{11}(\mathbf{r}))-1]+(\rho_1-\rho_2)^2 e^{-q_z^2\sigma_2^2}[\exp(q_z^2 C_{22}(\mathbf{r}))-1]$$
$$+2\rho_1(\rho_1-\rho_2)\cos(q_z d)e^{-q_z^2(\sigma_2^2+\sigma_1^2+\delta^2)}[\exp(q_z^2 C_{12}(\mathbf{r}))-1]\}e^{i\mathbf{q}_\perp\mathbf{r}}\ , \tag{3}$$

by rewriting the correlation function into two parts,

$$\exp\left[-\frac{q_z^2}{2}G_{ij}(\mathbf{r})\right]=\exp\left[-\frac{q_z^2}{2}(\sigma_i^2+\sigma_j^2)\right]+\exp\left[-\frac{q_z^2}{2}(\sigma_i^2+\sigma_j^2)\right][\exp(q_z^2 C_{ij}(\mathbf{r}))-1]\ , \tag{4}$$

where $C_{ij}(\mathbf{r})=\langle h_i(0)h_j(\mathbf{r})\rangle$. One may notice that the specular part is only sensitive to the rms values of the surface roughness, while the diffuse scattering profile contains information on the height fluctuations. The roughness of each interface contributes to the overall decay of the reflectivity independently, while the decay of the intensity oscillations was controlled collectively.

To apply Eq. (2) to describe the measured specular-reflectivity curve, the contribution from the diffuse part of the scattering has to be carefully measured and subtracted. We illustrated the measured diffuse scattering profile in Fig. 3 (the broken line) that was numerically added to Eq. (2) before fitting the specular reflectivity. In the fit, we also made appropriate corrections for the illuminated area, for the conversion factors in the reciprocal to the solid angle space mapping,[6] and for the x-ray absorption in the Au film. The best fit of the specular-reflectivity curve to Eq. (2) was obtained with $\sigma_1=8.5\pm1$ Å, $\sigma_2=5.5\pm1$ Å, and $\delta=2.7\pm0.7$ Å (illustrated by a solid line in Fig. 3). We attribute the roughness of the Au/GaAs interface, $\sigma_2=5.5$ Å to the combined effect of the atomic steps on the clean GaAs prior to the deposition,[11] and the interdiffusion of the Au and GaAs atoms at the interface. We note that the intermixing was minimal and confined to the first few contact monolayers. The surprisingly low intermixing at the interface may be a characteristic of a crystalline epitaxial Au film as opposed to polycrystalline films. Significant intermixing has been reported on polycrystalline Au films on GaAs through interfacial defects such as grain boundaries.[12] The roughness of air/Au interface, $\sigma_1=8.5$ Å was somewhat larger than σ_2. However, considering the fact that the sample had been exposed to air for an extended period of time, the air/Au surface was fairly smooth suggesting that the Au surface was very stable in air. Although σ_2 was only slightly smaller than σ_1, the overall intensity in the reflectivity curve above $q_2>0.2$ Å^{-1} was largely controlled by the roughness of the Au/GaAs interface since the specular reflectivity decays exponentially as the roughness increases. The overall figure error δ was also very small illustrating the effectiveness of the state of the art MBE growth technique.

IV. CORRELATED ROUGHNESS AND THE DIFFUSE SCATTERING

A surface of a thin (a few atomic layers thick) epitaxially grown film is generally expected to replicate the surface of the underlying substrate. In other words, the height fluctuations of the film surface are highly correlated to those of the film-substrate interface. As the thickness of an overlayer film increases, the correlation decreases. The correlation, quantified by $G_{12}(\mathbf{r})=\langle[h_1(\mathbf{r})-h_2(0)]^2\rangle$, is a good measure that indicates how much defect structures on the substrate, such as steps, islands, or some artificial structures propagate through an overlayer film. In this section, we present a scheme to obtain the correlated height fluctuations of the air/Au/GaAs system quantitatively from the diffuse part of the reflectivity curve.

The presence of the correlation between the interfacial height fluctuations was directly shown by the intensity oscillations in the longitudinal diffuse scattering, the diffuse scattering profile along the specular rod. The longitudinal diffuse scattering (shown in Fig. 3 by a broken line) was measured as a function of q_z at $q_x=3.3\times10^{-4}$ Å^{-1}, $q_y=0$ Å^{-1}, slightly off the specular rod. The position of measurement was close enough to the specular rod to obtain the peak intensity of the diffuse profile that has the transverse width of roughly $\Delta q_x=2\times10^{-3}$ Å^{-1} (HWHM), and was far enough to exclude the specular part of scattering completely in this high-resolution configuration. We note that the HWHM of the specular part limited by the instrumental resolution was as sharp as 5×10^{-5} Å^{-1}. The presence of the intensity oscillations in the diffuse scattering indicates that the interference term in Eq. (3) is nonzero, and the height fluctuations of the two interfaces are correlated, that is $C_{12}(\mathbf{r})\neq0$.[13]

The quantitative information of the correlated height fluctuations $G_{12}(\mathbf{r})=\langle[h_1(\mathbf{r})-h_2(0)]^2\rangle$ can be obtained from a detailed analysis of the transverse profile of the reflectivity. From Eq. (1), one may notice that a transverse profile, a $q_\perp$ scan at a fixed q_z, of a system with a single surface is just a Fourier transform of the quantity, $\exp[-(q_z^2/2)G(\mathbf{r})]$. The height fluctuations of a single surface system can be directly obtained by inverse-Fourier transforming the transverse scattering profile. It is, however, rather complicated to obtain the height fluctuations of a system with multiple interfaces, since the scattering profile has contributions from all interfaces and from the interference terms among them, as indicated in Eq. (1).

We start the analysis by noting that the intensity oscillations were much more rapid than any other variations in q_z. In a real-space picture, this means that the thick-

ness of the overlayer, ~1000 Å was much larger than any other length scales involved in the z direction such as the surface roughness that was only a few Å large. It is, therefore, possible to separate out the oscillatory term in Eq. (1) by taking the difference of the transverse profiles measured at an adjacent crest and valley of an oscillation,

$$S(\mathbf{q}_\perp, q_z^{\text{crest}}) - S(\mathbf{q}_\perp, q_z^{\text{valley}}) \approx F(q_z) \int d\mathbf{r}\, e^{-(q_z^2/2)G_{12}(\mathbf{r})} e^{i\mathbf{q}_\perp \cdot \mathbf{r}}, \quad (5)$$

where $F(q_z)$ is now only a function of q_z. Conveniently, the difference is just a two-dimensional Fourier transform of $\exp[-(q_z^2/2)G_{12}(\mathbf{r})]$. The measured profile was even simpler by the fact that the instrumental resolution was wide in the out of plane direction, $\hat{q}_y$ to allow an automatic integration over q_y,

$$\Delta I = I(q_x, q_z^{\text{crest}}) - I(q_x, q_z^{\text{valley}}) = G(q_z) \int dX\, e^{-(q_z^2/2)G_{12}(X)} e^{iq_x X}. \quad (6)$$

The difference of the measured intensity is a one-dimensional Fourier transform of $\exp[-(q_z^2/2)G_{12}(X)]$ that can be readily inverse-Fourier transformed to yield the correlated height fluctuations, $G_{12}(r)$.

To apply this scheme to obtain the $G_{12}(r)$, both the specular and the diffuse components of the scattering should be measured accurately with the instrumental effects deconvoluted. Although the diffuse and specular components might be measured simultaneously at low q_z, the dynamic scattering effects at small incident angles would complicate the scattering process,[8,14] which makes the analysis of the scattering profile in terms of the height fluctuations nearly impossible. We, instead, measured the transverse profile, q_x scan at $q_z = 0.33$ Å^{-1} (at crest) and $q_z = 0.334$ Å^{-1} (at valley) that were illustrated in Figs. 4(a) and 4(b). As illustrated in the figures, around $q_z = 0.33$ Å^{-1} the specular part of the scattering was dominated by the diffuse component. Even with the sharp resolution of 5×10^{-5} Å^{-1} (HWHM, including the surface mosaicity), the weak and infinitely sharp component was difficult to measure over the diffuse scattering, which was integrated over the entire resolution volume. For the specular component, we instead used the extrapolated value obtained from the fit of the specular reflectivity presented in the previous section. Since the extrapolated value was also convoluted with the resolution, a careful deconvolution of the instrumental effects was performed to obtain the intrinsic δ-specular component relative to the diffuse scattering. The intrinsic δ-specular component was then represented by an asymptotic Gaussian with infinitesimally small width and added to the empirical line shape best describing the difference of the diffuse profile. The solid line in Fig. 4(c) represents ΔI that was used in the inverse Fourier transform to obtain $\exp[-(q_z^2/2)G_{12}(r)]$ within a multiplication factor. The constant multiplication factor was later determined by taking the limiting value, $G_{12}(\infty) = \sigma_1^2 + \sigma_2^2$ with σ's obtained from the specular reflectivity.

The correlated height fluctuations $G_{12}(r)$ thus obtained is illustrated in Fig. 4(e). The small value of $\sqrt{G_{12}(0)} \approx 2.0$ Å suggests that the interfaces are fairly well correlated consistent with the well-defined intensity oscillations in the longitudinal diffuse scattering. We note that perfectly correlated interfaces where $h_1(r) \equiv h_2(r)$, would have $G_{12}(r) = G_{11}(r) = G_{22}(r)$, and $G_{12}(0) = 0$, while completely uncorrelated interfaces would have $\langle h_1(0)h_2(r)\rangle \equiv 0$ and $G_{12}(r) = \sigma_1^2 + \sigma_2^2$ for all r. The small value of $G_{12}(r)$ at the origin indicated that the interfacial correlation was quite good even though the overlayer was as thick as 1000 Å. This shows that the surface-height profile of the substrate was well kept during the process of growing the thick Au film. One may also notice that the interface correlation persisted rather long range in the lateral direction. Taking inverse of the half-width of the difference of the diffuse profile, was obtained the correlation length of about 1000 Å.

Similarly, one might expect to obtain some insight on the height fluctuations, $G_{11}(r)$ and $G_{22}(r)$ by adding the

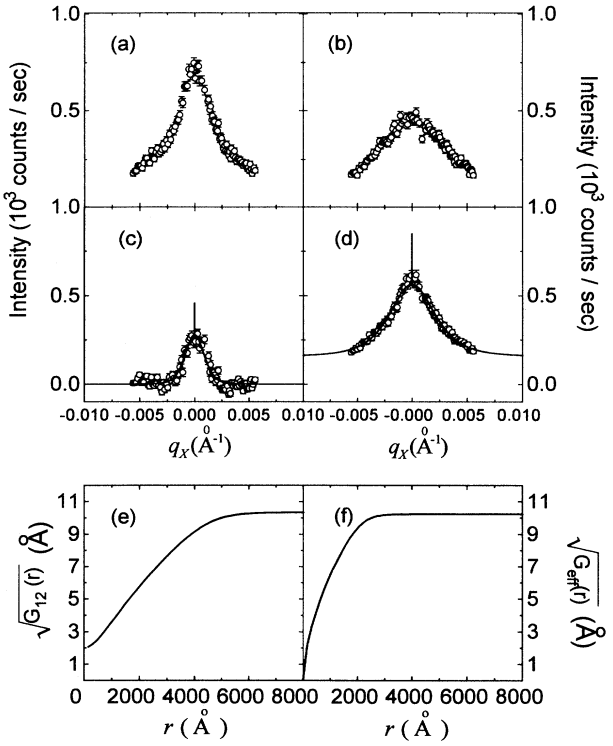

FIG. 4. (a) The measured transverse, q_x scan at $q_z = 0.33$ Å^{-1}, at a crest of the intensity oscillations. (b) The q_x scan at $q_z = 0.334$ Å^{-1}, at a valley of the intensity oscillations. (c) The difference of the intensity profiles at the crest and at the valley. The solid line is the best fit to the difference profile with the extrapolated δ-specular component added. (d) The sum of the intensity profiles at the crest and at the valley. The solid line is the best fit to the average profile with the extrapolated δ-specular component added. The data and the fit are multiplied by a factor of 0.5 for a clear illustration. (e) Square root of the correlated height-fluctuation function, $G_{12}(\mathbf{r}) = \langle [h_i(\mathbf{r}) - h_j(0)]^2 \rangle$ obtained by an inverse Fourier transform of the difference profile. $\sqrt{G_{12}(0)} \approx 2$ Å was not zero, but small indicating the interfaces were well correlated. (f) Square root of the effective height-fluctuation function as defined in the text.

diffraction profile at the peak and at the valley, and eliminating the oscillatory term in Eq. (1),

$$S(\mathbf{q}_\perp, q_z^{\text{crest}}) + S(\mathbf{q}_\perp, q_z^{\text{valley}}) = H(q_z) \int d\mathbf{r} \left[e^{-(q_z^2/2)G_{22}(\mathbf{r})} + \frac{\rho_{\text{Au}}^2}{(\rho_1 - \rho_2)^2} e^{-(q_z^2/2)G_{11}(\mathbf{r})} \right] e^{i\mathbf{q}_\perp \cdot \mathbf{r}} . \tag{7}$$

Unfortunately, it is not straightforward to obtain $G_{11}(r)$ or $G_{22}(r)$ separately by inverting this equation because the integrand is a sum of the two independent terms. Only when one of the interfaces is much rougher than the other, it is possible to ignore the corresponding term, and to obtain the height-fluctuation profile of the other term. In Fig. 4(d), we represent the sum of the measured scattering profile together with the best-fit solid line that includes the specular component as well. By approximating the integrand in Eq. (7) as,

$$e^{-(q_z^2/2)G_{\text{eff}}(\mathbf{r})} = e^{-(q_z^2/2)G_{22}(\mathbf{r})} + \frac{\rho_{\text{Au}}^2}{(\rho_1 - \rho_2)^2} e^{(q_z^2/2)G_{11}(\mathbf{r})} , \tag{8}$$

and applying a similar algebra as for $G_{12}(r)$, we obtained the effective height fluctuations, $G_{\text{eff}}(r)$ that are represented in Fig. 4(f).

The procedure developed above may be applied to the transverse scans taken at various values of q_z to yield the same results for $G_{12}(r)$ and $G_{\text{eff}}(r)$. Although this will provide a valuable check for the validity of the procedure, it was not possible in this experiment. At q_z's less than 0.2 Å^{-1}, the dynamic scattering effect was not negligible as mentioned before, and at values larger than 0.4 Å^{-1} the scattering intensity above the background was too small for any meaningful analysis. We believe that one may apply the procedure at various q_z's on other systems.

V. SATELLITE PEAKS IN THE ROCKING CURVES AT SMALL q_z

It is well known that the kinematic approximation used in Eq. (1) breaks down at low incident angles due to the dynamic scattering effects.[14] One of the most well-known effects is the Yoneda wing, four-fold enhancement of scattering intensity at incident angle or exit angle at the critical angle of an interface.[15] For incident angles less than the critical angle, the total external reflection occurs. The value of the critical angle depends on both the incident x-ray energy and the difference of the electron density across the interface. In this section, we discuss an observation of enhancement of the scattering intensity in rocking curves (transverse scans) due to the dynamic scattering effects and the correlated roughness of the interface.

In Fig. 5(a), a pair of rocking curves (at a crest, $q_z = 0.151$ Å^{-1} and at a nearby valley, $q_z = 0.154$ Å^{-1}) of the specular reflectivity are illustrated. Each curve was taken by rocking the sample at the detector angle, Θ, fixed to a specific value. They are plotted against both the in-plane momentum transfer and the incident angle. One may immediately notice that there are extra satellite peaks in addition to the Yoneda wings. The Yoneda wings were associated to the air/Au interface, and occurred at 0.39° of incident (or exit) angle consistent with the calculated critical angle. We note that the total external reflection does not occur at the Au/GaAs interface since the Au electron density is larger than the GaAs electron density. As a consequence, there are no Yoneda wings associated to the buried Au/GaAs interface.

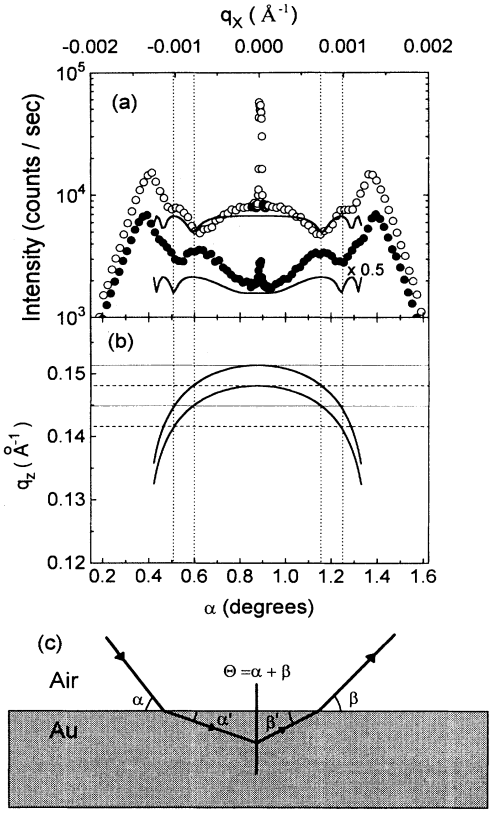

FIG. 5. (a) Rocking curves measured at a crest, $q_z = 0.15$ Å^{-1} (open circles) and at a nearby valley, $q_z = 0.153$ Å^{-1} (solid circles). The scattering profile at the valley was multiplied by a factor of 0.5 for a clear illustration. One may easily notice the extra satellite peaks as well as the Yoneda wings. The solid lines are to illustrate the maxima of the interference factor $\sim\cos(q_z d)$ scaled by arbitrary factors. (b) The thick solid lines represent the change of the q_z component in the course of the rocking curves. The positions of the maxima of $\sim\cos(q_z d)$ are indicated by the thin solid lines, while the minima of $\sim\cos(q_z d)$ are indicated by the thin broken lines. We also drew dotted lines to indicate the satellite-peaks positions at the maxima of $\sim\cos(q_z d)$ through (a) and (b). (c) A schematic representation of the path of x rays across the air/Au interface. The incident and exit angles in Au are related to those in air by Eq. (9).

To understand the origin of the additional satellite peaks, we point out several features associated with them. They are symmetrically located from the main specular peak indicating that they occur when the incident or the exit angle satisfies a common condition. It is clear that they are not due to any simple critical-angle enhancement at a fixed angle of incidence, since the incident angle at the satellite peaks varies with q_z. They are also not originated from any periodic in-plane modulation as clearly indicated by the difference in the peak position in q_x between the rocking curves at the crest from that at the valley of q_z. In the rocking curve at the valley, the satellite peaks move in toward the specular rod. The large change in the satellite-peak position as q_z varies from the crest to the valley suggests that they might be related to the interference term in Eq. (1).

The incident (or exit) angle at the satellite peaks was very small, less than 1°. At this small incident angle, the path of x rays in Au deviates significantly from that in the air as a consequence of the dynamic scattering effects. A full treatment of the electromagnetic waves in a medium or at least a distorted-wave Born approximation is required to explain the scattering profile quantitatively.[8] In this section, we try to investigate the physical origin that describes the existence of the satellite peaks qualitatively.

In Fig. 5(c), we illustrated schematically the actual path of the x rays in Au using Snell's law,[16]

$$\cos(\alpha')=\frac{1}{n}\cos(\alpha), \quad n=\left[1-\frac{4\pi\rho_{\mathrm{au}}^2}{m\bar{\omega}^2}\right]^{1/2}, \tag{9}$$

where α is the incident angle in air, α' is the refracted angle in Au, n is the index of refraction at the air/Au interface, m is the electron mass, $\bar{\omega}$ is the angular frequency of the radiation, and ρ_{au} is the change density of the Au film. Clearly, the momentum transfer calculated in air, would be different from that in Au. Specifically for a given scattering angle Θ (in the air) the momentum transfer is given by,

$$\begin{aligned} &q_z^{\mathrm{air}}=k(\sin\alpha+\sin\beta), \quad q_x^{\mathrm{air}}=k(\cos\alpha-\cos\beta) \\ &q_z^{\mathrm{au}}=nk\left[\left[1-\frac{\cos^2\alpha}{n^2}\right]^{1/2}+\left[1-\frac{\cos^2\beta}{n^2}\right]^{1/2}\right], \\ &q_x^{\mathrm{au}}=nk\left[\frac{\cos\alpha}{n}-\frac{\cos\beta}{n}\right] \quad \text{with } \beta=\Theta-\alpha\ . \end{aligned} \tag{10}$$

Obviously, the q_z component of the momentum transfer in Au changes substantially as the incident angle approaches to the critical angle, while it remains nearly constant in air. Therefore, the rocking curve follows a quite different path in the reciprocal space from a pure transverse scan where the q_z component of the momentum transfer is fixed. The change of q_z in the rocking curves is illustrated in Fig. 5(b).

We believe that the origin of the satellite peaks is closely related to the change of q_z in the course of the rocking curves, since the diffuse scattering as well as the specular reflectivity oscillates as a function of q_z due to the correlated height fluctuations of the interfaces. In a rocking curve, since the q_z component of momentum transfer in Au changes as described above, the intensity profile would be modulated by the interference term $\sim\cos(q_z d)$ in Eq. (1). In fact, Fig. 5(b) shows that the change in q_z is large enough that the interference term changes from the maxima to the minima. Therefore, a satellite feature occurs whenever the interference term in Eq. (1), $\sim\cos(q_z d)$ becomes a maximum. The interference term, $\cos(q_z d)$ with an appropriate scale factor is drawn in Fig. 5(a) to illustrate the positions of the maxima that are well matched to the satellite-peak position. The good agreement in both the rocking curves suggests that the satellite peaks were originated from the actual path of the x rays in Au and the correlated roughness of the interfaces that induces the oscillations in the diffuse scattering.

VI. ANNEALING AND THE INTERDIFFUSION

Finally, we heat up the sample to 400 °C extensively (> 5 h) to observe possible changes in the interfacial structure. As summarized in Fig. 6, the specular

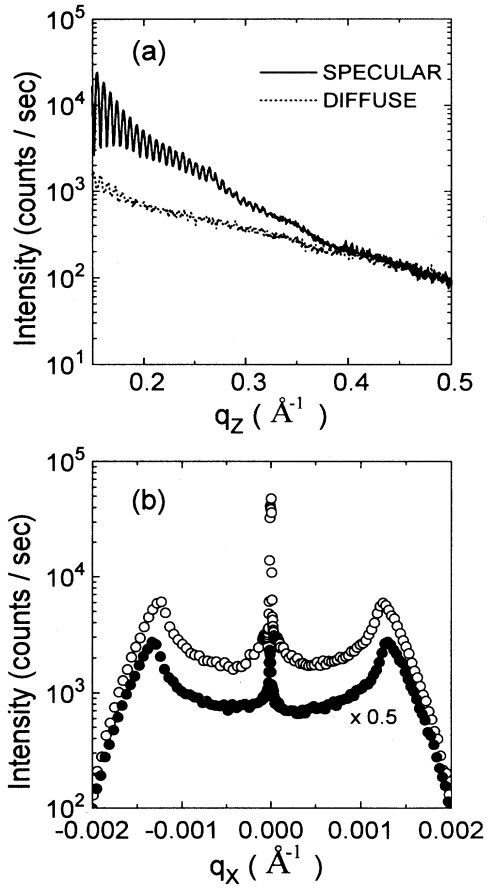

FIG. 6. (a) The specular reflectivity (solid line) and the longitudinal diffuse scattering (dotted line) after annealing the sample to 400 °C. (b) The rocking curves measured at a crest, $q_z=0.151$ Å^{-1} (open circles) and at a nearby valley, $q_z=0.154$ Å^{-1} (solid circles) after annealing. Notice that no satellite peaks are present.

reflectivity and the diffuse scattering profile have changed significantly after annealing. First, the intensity of the specular reflectivity was significantly decreased indicating the interfaces, especially the buried Au/GaAs interface became rougher. Second, the intensity oscillations in the longitudinal diffuse scattering represented by the dotted line became very weak or disappeared. This suggests that the correlation of the height fluctuations between the two interfaces was lost. At the same time, as shown in Fig. 6(b), the satellite peaks in the rocking curves at small incident angles disappeared as well. This is likely due to the loss of the interfacial correlation that destroys the intensity oscillations in the diffuse scattering profile. The concurrent disappearance of the satellite peaks and the interfacial correlation was consistent with the model for the satellite peaks presented in the previous section.

We believe that the changes at the elevated temperature were due to the interdiffusion of atoms occurred at the Au/GaAs interface. The small intensity modulation on top of the rapid intensity oscillations [see Fig. 6(a)] in the specular-reflectivity curve suggests that there is a layer with density different from both Au and GaAs. From the period of the modulation, we estimate that the thickness of this layer is about 60 Å. We attribute this layer to the intermixing of the atoms across the Au/GaAs interface. A systematic study of the interdiffusion across the crystalline Au/GaAs interface at elevated temperatures will be performed in the future.

VII. CONCLUDING REMARKS

In this paper, we demonstrated the capability of x-ray reflectivity in studying the interfacial structures of a thin Au crystalline film epitaxially grown on GaAs. The specular-reflectivity curve was analyzed to obtain the roughness of the buried Au/GaAs interface (5 Å) and the air/Au interface (8 Å). The well-defined Au/GaAs interface indicated that the interdiffusion was minimal at room temperature. The regular intensity oscillations suggested that the film thickness was uniform in atomic scale across the whole illuminated area. The height fluctuations of the interfaces were highly correlated as illustrated by the regular intensity oscillations in the longitudinal diffuse profile. We obtained the correlated height fluctuations, $G_{12}(\mathbf{r})=\langle[h_1(\mathbf{r})-h_2(0)]^2\rangle$ quantitatively by comparing the diffuse profile at the crest of an oscillation to that at the valley. The correlated height fluctuations were also manifested by the newly discovered satellite peaks at low incident angles. The satellite peaks were consistently explained by the dynamic scattering effects and the intensity oscillations in the diffuse scattering due to the correlated roughness.

The interfacial structure was drastically modified after annealing the sample at 400 °C for a few hours. The specular-reflectivity intensity was sharply declined indicating that the buried Au/GaAs interface became rough. As the same time the interfacial correlation was diminished sharply as suggested by the disappearance of the intensity oscillations in the diffuse scattering and the satellite peaks. We believe that these changes were caused by the intermixing of atoms at elevated temperatures.

ACKNOWLEDGMENTS

We hope that this study provides a stepping stone in applying x-ray reflectivity study for characterizing interfacial structures of thin films. We gratefully acknowledge K. S. Liang and S. K. Sinha for valuable discussions. We also express our thanks to Z. Fu and J. H. Je for their valuable contribution in the synchrotron measurement, and to J. P. Mannaerts for his efforts in the preparation of the Au/GaAs film. One of the authors, H. K. Kim acknowledges the support from Pohang Light Source and RCDAMP in Korea.

[1]Z. Lilental-Weber, R. Gronsky, J. Washburn, N. Newman, W. E. Spicer, and E. R. Weber, J. Vac. Sci. Technol. B **4**, 912 (1986).

[2]T. Okumura and K. N. Tu, J. Appl. Phys. **61**, 2955 (1987).

[3]L. G. Parratt, Phys. Rev. **95**, 359 (1954); S. R. Andrew and R. A. Cowley, J. Phys. C **18**, 6427 (1985).

[4]R. A. Cowley and T. W. Ryan, J. Phys. D **20**, 61 (1987).

[5]A. Braslau, M. Deutsch, P. S. Pershan, A. H. Weiss, J. Als-Nielsen, and J. Bohr, Phys. Rev. Lett. **54**, 114 (1985).

[6]S. K. Sinha, E. B. Sirota, S. Garoff, and H. B. Stanley, Phys. Rev. B **38**, 2297 (1988).

[7]S. K. Sinha, M. K. Sanyal, S. K. Satija, C. F. Majkzak, D. A. Neumann, H. Homma, S. Szpala, A. Gibaud, and H. Morkoc, Physica B **198**, 77 (1994).

[8]V. Holy and T. Baumbach, Phys. Rev. B **49**, 10 668 (1994).

[9]R. L. Headrick and J. M. Baribeau, Phys. Rev. B **48**, 9174 (1993).

[10]M. Hong, J. P. Mannaerts, L.H. Grober, S. N. G. Chu, H. S. Luftman, K. D. Choquette, and R. S. Freund, J. Appl. Phys. **27**, 3105 (1994).

[11]E. J. Heller, Z. Y. Zhang, and M. G. Lagally, Phys. Rev. Lett. **71**, 743 (1993).

[12]V. G. Weizer and N. S. Fatemi, J. Appl. Phys. **64**, 4618 (1988).

[13]R. Pynn, Phys. Rev. B **45**, 602 (1992).

[14]G. H. Vineyard, Phys. Rev. B **26**, 4146 (1982), and references therein.

[15]Y. Yoneda, Phys. Rev. **131**, 2010 (1963).

[16]J. D. Jackson, *Classical Electrodynamics* (Wiley, New York, 1975), Chap. 7.